GEOPHYSICAL RESEARCH LETTERS, VOL. 32, L24818, doi:10.1029/2005GL024074, 2005

Why the melting layer radar reflectivity is not bright at 94 GHz

Pavlos Kollias[1] and Bruce Albrecht[2]

Received 18 July 2005; revised 29 September 2005; accepted 9 November 2005; published 31 December 2005.

[1] At 94 GHz, the highest radar frequency used for atmospheric research, no radar bright band is observed at the melting layer. In this study, simulations of a vertical profile of melting particles and their scattering properties for a variety of melting particle models are used to capture the basic features of the radar reflectivity structure at 94 GHz in the melting layer. Observations of stratiform precipitation from vertically pointing 3 GHz and 94 GHz radars are used for comparison with the model results. The simulations show good agreement with the observations. The melting of precipitating particles results in an abrupt increase in the radar reflectivity at 94 GHz without a subsequent decrease at the base of the melting layer. The simulations also captured a small decrease in the radar reflectivity at 94 GHz (dark band) often observed at the top of the melting layer.
Citation: Kollias, P., and B. Albrecht (2005), Why the melting layer radar reflectivity is not bright at 94 GHz, *Geophys. Res. Lett.*, *32*, L24818, doi:10.1029/2005GL024074.

1. Introduction

[2] Early observations of stratiform rain from centimeter wavelength radars [e.g., *Battan*, 1973] revealed an area of enhanced radar reflectivity near the 0°C isotherm. The enhancement of the radar reflectivity at the melting layer has captured the interest of radar meteorologists since the early days of radar meteorology [e.g., *Austin and Bemis*, 1950; *Aden and Kerker*, 1951; *Lhermitte and Atlas*, 1963]. The reflectivity enhancement was attributed to the melting of snowflakes and their conversion to raindrops, particles with higher dielectric constant. Furthermore, the increase of the fall velocity of the melted particles induces a reduction in the number density of particles (divergence) below the region of enhanced reflectivity and a small drop of the radar reflectivity. The shallow layer of enhanced reflectivity extends about 500–700 m below the 0°C isotherm level and it is called the radar bright band.

[3] The shape and intensity of the radar bright band is related to the shape and number concentration of the ice crystals and snowflakes above the melting layer, the melting rate of the snowflakes, the maximum size of melted particle, and the rainfall intensity. But there has been no real appreciation of how radar wavelength influences the final shape of the radar reflectivity profile in the melting layer. This is exemplified by 94 Ghz radars that use the shortest wavelength available for meteorological applications.

[4] At 94 GHz, no radar bright band is observed at the melting layer (Figure 1). A sharp increase of the radar reflectivity is observed without a subsequent decrease at lower height. Often, at low rainfall rates, a small decrease (1–2 dBZ) of the radar reflectivity (dark band) is observed first, just below the 0°C isotherm, before the sharp increase of the radar reflectivity is observed. Overall, the 94 GHz radar profile at the melting layer can be described as a sharp reflectivity jump [e.g., *Sassen et al.*, 2005]. With the growing interest in the use of 94 GHz Doppler radars from several research programs, such as the Atmospheric Radiation Measurements Program [*Widener and Mead*, 2004], CloudSat [*Stephens et al.*, 2000] and NCAR's High-performance Instrumented Airborne Platform for Environmental Research (HIAPER) for the study of clouds and precipitation, there is a need for an accurate representation of the melting layer at such high radar frequencies.

[5] The aim of this study is to provide a comprehensive understanding of the 94 GHz radar profile in the melting layer (Figure 1) through the use of a melting layer model and comparisons with collocated observations from vertically pointing 94 and 3 GHz radars in stratiform rain. We are particularly interested in explaining the lack of a reflectivity decrease at 94 GHz at the base of the melting layer and investigating the conditions that lead to the development of a shallow dark band at 94 GHz near the top of the melting layer.

2. Modeling of the Melting Layer

[6] Modeling efforts on the melting layer of precipitation abound in the literature, from one-dimensional models [e.g., *Klaassen*, 1988; *D'Amico et al.*, 1998], to two-dimensional [*Szyrmer and Zawadski*, 1999] to Doppler spectra models [*Skaropoulos and Russchenberg*, 2003]. Our aim is to analyze the radar reflectivity profile of the melting layer, not the development of a new physical model of melting snowflakes. Thus, the physical model described by *Szyrmer and Zawadski* [1999] is used to provide the vertical profile of the melting hydrometeors needed for the radar reflectivity forward model. The melting of snowflakes occurs in a shallow (500–700 m) layer below the 0°C isotherm where snowflakes melt and turn into raindrops. Above the melting layer (T < 0°C), snowflakes are modeled as a mixture of ice and air (ice inclusions in an air matrix), and the density of the snow determines the volume fraction f of the ice in the air. In our study, the $p_s(D_s) = 0.015 D_s^{-1}$ [*Mitchell et al.*, 1990] was selected to describe the relationship of snow density p_s to the diameter of the snowflake D_s. In the melting layer, a mixture of partially melted snow particles and raindrops exist. The shape of particles during melting is highly variable [e.g., *Willis and Heymsfield*, 1989]. In our study we have adopted three different melting snowflake models from *Fabry and Szymer* [1999]. In Model 1, the

[1]Atmospheric Science Department, Brookhaven National Laboratory, Upton, NY, USA.
[2]Rosenstiel School of Marine and Atmospheric Sciences, University of Miami, Miami, FL, USA.

0094-8276/05/2005GL024074$05.00

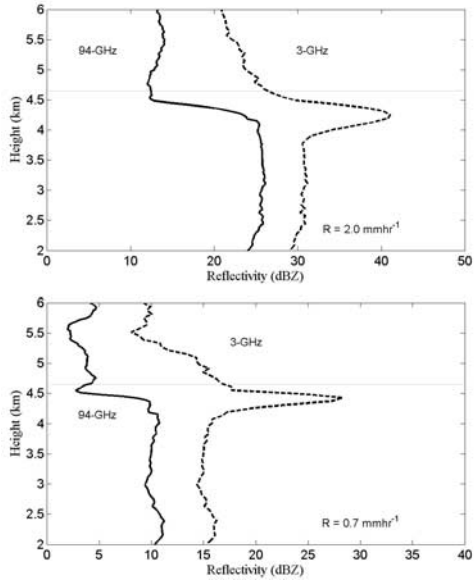

Figure 1. Observed profiles of radar reflectivity at 3 GHz (dotted line) and 94 GHz (solid line) in stratiform precipitation. The 0°C isotherm is located at 4.6 km and the surface rainfall rate is (top) 2 $mmhr^{-1}$ and (bottom) 0.7 $mmhr^{-1}$. The 94 GHz radar reflectivity profile below the melting layer (only raindrops) has been corrected for Mie effects and attenuation using the corresponding 3 GHz radar reflectivity values and offset for clarity.

melting hydrometeor is composed of ice inclusions in an air matrix (snow) in a water matrix, ([[[ice], air], water]). In Model 2, the melting hydrometeor is composed of ice inclusions in a water matrix in an air matrix, ([[[ice], water], air]). Finally in Model 3, the melting hydrometeor is composed of air inclusions in a matrix composed by a mixture of ice inclusions in a water matrix, ([air, [[ice], water]]).

[7] For each melting hydrometeor model, the average dielectric constant of the uniform mixture (inclusion-matrix) is derived by the Maxwell Garnett formula [*Maxwell Garnett*, 1904; *Bohren and Battan*, 1982; *Meneghini and Liao*, 2000]. Once the dielectric constant of the spherical melting snowflakes is specified at each height in the melting layer, the Mie scattering solution is used to calculate their scattering characteristics.

3. Results

[8] In July 2002, NASA's CRYSTAL-FACE experiment for the study of tropical cirrus anvils took place in South Florida. During the experiment, the NOAA Aeronomy Laboratory 3 GHz profiler and the University of Miami 94 GHz Doppler cloud radar were collocated at a ground site 40 km southwest of Miami Florida. Radar observations of the melting layer during a weak stratiform precipitation even at 94 GHz (Figure 1) revealed the absence of an area of enhanced reflectivity (bright band), the presence of a sharp increase in the reflectivity, and often the presence of a reflectivity minimum (dark band) at the top of the melting layer. Figure 2 shows the simulated radar reflectivity and attenuation at 94 GHz (top) for an exponential raindrop size distribution [*Marshall and Palmer*, 1948], a surface rainfall rate of 1 $mmhr^{-1}$ and for all three melting snowflake models. For comparison, the corresponding profiles at 3 GHz are shown (Figure 2 (bottom)). The simulations (Figure 2) are in good agreement with the observations and capture the main features of the observed radar reflectivity profile at 94 GHz and 3 GHz (Figure 1). At 3 GHz the melting layer ends at the depth of 630 m below the 0°C isotherm where the largest snowflake in the physical model completely melts to a spherical raindrop with 4 mm diameter. This feature of the radar reflectivity profile is similar to the observed 3 GHz radar reflectivity profile. At 94 GHz the reflectivity profile is invariant below 250 m depth. The maximum attenuation simulated at 94 GHz in the melting layer is between 1.5–2.2 $dBkm^{-1}$ among the different melting snowflake models used, while attenuation in the liquid layer is 1.3 $dBkm^{-1}$. When averaged over the depth of the melting layer, the 94 GHz radar signal attenuation is comparable to the attenuation in the liquid layer below the melting layer. This is not the case at 3 GHz, where signal attenuation in the melting layer is much stronger than it is in the liquid layer (Figure 2).

[9] At 3 GHz the contribution to the radar reflectivity from any raindrop is proportional to D^6. As a result, a few large raindrops in the radar resolution volume contribute to the Doppler moments as much as thousands of small raindrops. This is not accurate in 94 GHz radars since the backscattering cross section for raindrops is not proportional to the sixth power of the raindrop diameter [*Kollias et al.*, 2002]. Figure 3 shows the contribution to the reflectivity profiles of Figure 2 from four raindrop size ranges: 0–1 mm, 1–2 mm, 2–3 mm and 3–4 mm for a Marshall-Palmer

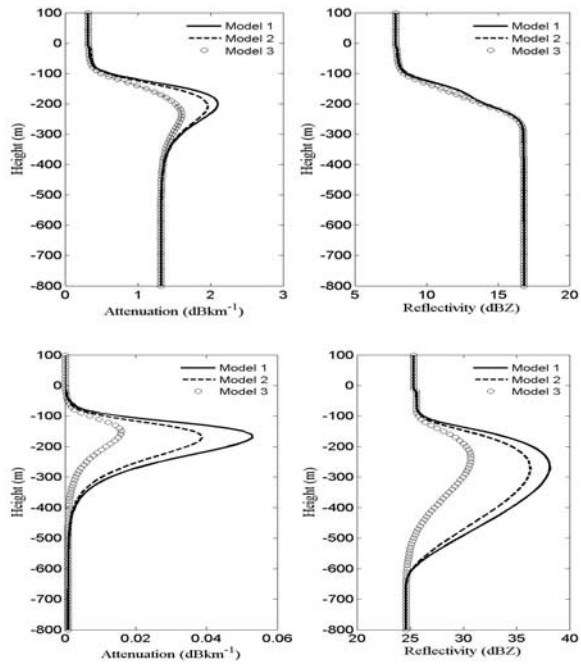

Figure 2. Simulated profiles of radar reflectivity and attenuation at (top) 94 GHz and (bottom) 3 GHz for three different models of melting snowflakes (Fabry and Szyrmer, 1999) for a Marshall-Palmer raindrop size distribution and 1 $mmhr^{-1}$ surface rainfall rate.

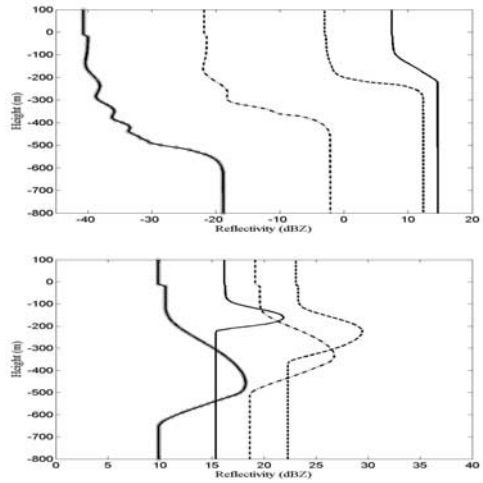

Figure 3. Vertical profiles of radar reflectivity at (top) 94 GHz and (bottom) 3 GHz contribution from four raindrop size ranges: 0–1 mm (solid), 1–2 mm (dashed), 2–3 mm (dash-dotted) and 3–4 mm (diamonds) for a Marshall-Palmer size distribution and 1 mm hr^{-1} surface rainfall rate.

exponential size distribution [*Marshall and Palmer*, 1948] and 1 $mmhr^{-1}$ rainfall rate. At 94 GHz the group of raindrops with diameter less than 1 mm is the dominant contributor to the shape of radar profile shown in Figure 2. The complete melting of the snowflake that turns into a 1 mm diameter raindrop occurs at 230 m depth and beyond this point the reflectivity profile at 94 GHz remains constant. Despite the melting of larger snowflakes and the creation of larger raindrops deeper in the melting layer, their contribution to the reflectivity profile is not significant due to the exponential drop of their number concentration [*Marshall and Palmer*, 1948]. Thus there is no further increase of the reflectivity beyond the depth where the contribution from relatively small raindrops overwhelms

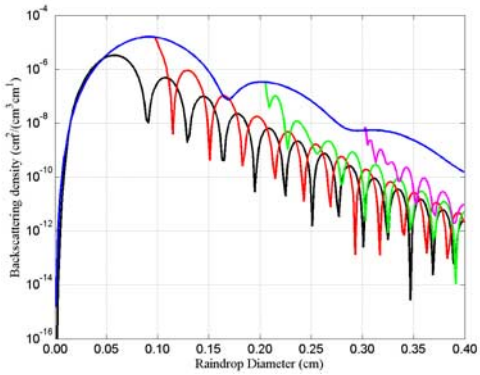

Figure 4. Backscattering cross sections of hydrometeors multiplied by their number concentration at various depths in the melting layer as a function of their equivalent raindrop diameters. Top of the melting layer, no melting (black line), depth where 1 mm raindrops form (red), depth where 2 mm raindrops form (green), depth where 3 mm raindrops form (magenta) and base of the melting layer with all liquid raindrops (blue line).

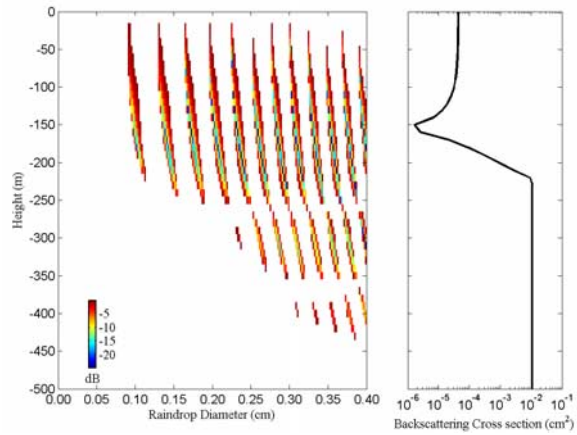

Figure 5. Mapping of the parameter $10\log_{10}[cb_{min}(D)/cb_{snowflake}(D)]$, where $cb_{min}(D)$ is the minimum simulated backscattering cross section of a particle with melted diameter D and $cb_{snowflake}(D)$ is the simulated backscattering cross section of the snowflake above the melting layer whose melted diameter is D. The colored areas indicate depth and diameter ranges where the melted particle has lower backscattering cross section that its corresponding snowflake particle. The white area indicates depth and diameter ranges where the backscatter cross-section of the melting particle is higher than the backscattering cross section of its corresponding snowflake above the melting layer. The backscattering cross section of a melting snowflake with melted diameter 1 mm is shown on the right.

the contribution from larger raindrops. Furthermore, there is no noticeable decrease in the reflectivity near the base of the melting layer when the fast falling large raindrops induce a reduction in the number of particles. This is not the case at 3 GHz. The contribution to reflectivity from larger raindrops generated by the complete melting of snowflakes deep in the melting layer is proportional to D^6 and this strong dependence overcomes the exponential drop in the number concentration. Thus, the overall effect is a significant contribution to the reflectivity profile from group of large raindrops deep in the melting layer (Figure 3 (bottom)) that affect the final shape of the reflectivity profile and are responsible for the presence of the radar bright band.

[10] Another interesting feature observed in Figure 1 is the presence of a shallow reflectivity minimum (dark band) just below the 0°C isotherm. The examination of a large data set of 94 GHz radar observations of stratiform precipitation demonstrated that this narrow dark band is more pronounced during weak rainfall rates (less than 1 $mmhr^{-1}$). The melting layer simulations in Figure 2, however, show no evidence of a reflectivity minimum just below the 0°C isotherm.

[11] During the melting process, there are two competing mechanisms that contribute to the backscattering cross section of melting snowflakes: The decrease of the diameter, due to the collapse of the low-density snowflake to a raindrop, decreases the backscattering, while the increase of the dielectric constant of the hydrometeor due to the presence of more water in the liquid phase, increases the

backscattering. Melting snowflakes have sizes comparable to the short wavelength ($\lambda = 3.2$ mm) at 94 GHz radars and the backscattering cross section at this frequency as a function of diameter exhibits a quasi-periodic form with an exponential damping of the oscillation (Figure 4). The oscillating nature of the backscattering curve is caused by the superposition of the multiple terms described in the Mie scattering solution. Figure 4 shows the backscattering cross section of hydrometeors for snowflake model 3 multiplied by their number concentration at various depths in the melting layer. It is apparent from Figure 4 that certain sizes of snowflakes will undergo decreases in their backscattering cross section per unit of volume during the melting process before they melt completely. Such behavior is evident for raindrops with diameters larger than 0.7 mm for certain size ranges of raindrops. Figure 5 shows the parameter $10\log_{10}[cb_{min}(D)/cb_{snowflake}(D)]$, where $cb_{min}(D)$ is the minimum simulated backscattering cross section of a particle with melted raindrop diameter D and $cb_{snowflake}(D)$ is the simulated backscattering cross section of a snowflakes above the melting layer whose melted raindrop diameter is D. The backscattering minima occur near the top of the melting layer, which is in good agreement with the observations (Figure 5). Small raindrops ($D < 0.8$ mm) do not contribute to the dark band. In contrast, small raindrops form near the top of the melting layer and contribute to the large reflectivity increase observed and simulated (Figure 2). Thus, these ''localized'' in diameter size and melting layer depth minima in the backscattering cross section can affect the reflectivity profile near the top of the melting layer if small raindrops are in low concentrations.

4. Summary

[12] At 94 GHz, no radar bright band is observed. The melting of precipitating particles results in an abrupt increase in the radar reflectivity without a following decrease at the base of the melting layer. In addition, a small decrease of the radar reflectivity (dark band) is often observed near the top of the melting layer. We investigated the scattering mechanism responsible for the observed structure of the 94 GHz radar reflectivity profile in the melting layer. The simulations presented in this study are in good agreement with the observations and capture the main features of the 94 GHz radar reflectivity profile in the melting layer. Small raindrops that are generated first, near the top of the melting layer through the melting of their corresponding snowflakes, have an overwhelming effect on the reflectivity profile, contrary to the insignificant effect of small raindrops to the final shape of lower radar frequency reflectivity profiles. Furthermore, during melting, certain size groups of snowflakes undergo a decrease of their backscattering cross section, and if their concentration relative to the other snowflakes is high, a dark band is produced near the top of the melting layer. Overall, low concentrations of small raindrops ($D < 1$ mm) are required for the generation of the radar dark band. The results from this study will improve our understanding of the melting layer radar signature at high radar frequencies, a critical issue for the development of new precipitation retrieval techniques from ground or space using cloud radars.

[13] **Acknowledgments.** This manuscript has been authored by Brookhaven Science Associates, LLC under Contract DE-AC02-98CH1-886 with the U.S. Department of Energy. This work was supported by NASA CRYSTAL-FACE Grant NAG511508 and NSF ATM 0201072.

References

Aden, A. I., and M. Kerker (1951), Scattering of electromagnetic waves by two concentric spheres, *J. Appl. Phys.*, *22*, 1242–1246.

Austin, P. M., and A. C. Bemis (1950), A quantitative study of the ''bright band'' in radar precipitation echoes, *J. Meteorol.*, *7*, 145–151.

Battan, L. J. (1973), Radar Observations of the Atmosphere, 325 pp., Univ. of Chicago Press, Chicago, Ill.

Bohren, C. F., and L. J. Battan (1982), Radar backscattering of microwaves by spongy ice spheres, *J. Atmos. Sci.*, *39*, 2623–2628.

D'Amico, M., A. R. Holt, and C. Capsoni (1998), An anisotropic model of the melting layer, *Radio Sci.*, *33*, 535–552.

Fabry, F., and W. Szymer (1999), Modeling of the melting layer. Part II: Electromagnetic, *J. Atmos. Sci.*, *56*, 3593–3600.

Klaassen, W. (1988), Radar observations and simulations of the melting layer of precipitation, *J. Atmos. Sci.*, *45*, 3741–3753.

Kollias, P., B. A. Albrecht, and F. D. Marks Jr (2002), Why Mie? Accurate observations of vertical air velocities and rain drops using a cloud radar, *Bull. Am. Meteorol. Soc.*, *83*, 1471–1483.

Lhermitte, R. M. and D. Atlas (1963), Doppler fall speed and particle growth in stratiform precipitation, paper presented at Tenth Weather Radar Conference, Am. Meteorol. Soc., Boston, Mass.

Marshall, J. S., and W. H. Palmer (1948), The distribution of raindrops with size, *J. Meteorol.*, *5*, 165–166.

Maxwell Garnett, J. C. (1904), Colours in metal glasses and in metallic films, *Philos. Trans. R. Soc. London, Ser. A*, *203*, 385–420.

Meneghini, R., and L. Liao (2000), Effective dielectric constants of mixed-phase hydrometeors, *J. Atmos. Oceanic. Technol.*, *17*, 628–640.

Mitchell, D. L., R. Zhang, and R. L. Pitter (1990), Mass-dimensional relationships for ice particles and the influence of riming on snowfall rates, *J. Appl. Meteorol.*, *29*, 153–163.

Sassen, K., J. R. Campbell, J. Zhu, P. Kollias, M. Shupe, and C. Williams (2005), Lidar and triple-wavelength Doppler radar measurements of the melting layer: A revised model for dark- and brightband phenomena, *J. Appl. Meteorol.*, *44*, 301–312.

Skaropoulos, N. C., and H. W. J. Russchenberg (2003), Simulations of Doppler spectra in the melting layer of precipitation, *Geophys. Res. Lett.*, *30*(12), 1634, doi:10.1029/2003GL016959.

Stephens, G. L., et al. (2002), The CLOUDSAT mission and the A-train, *Bull. Am. Meteorol. Soc.*, *83*, 1771–1790.

Szyrmer, W., and I. Zawadski (1999), Modeling of the melting layer. Part I: Dynamics and microphysics, *J. Atmos. Sci.*, *56*, 3573–3592.

Widener, K. B. and J. B. Mead (2004), W-band ARM cloud radar-specifications and design, paper presented at Fourteenth ARM Science Team Meeting, Atmos. Rad. Meas. Program, Albuquerque, N. M.

Willis, P. T., and A. J. Heymsfield (1989), Structure of the melting layer in mesoscale convective system stratiform precipitation, *J. Atmos. Sci.*, *46*, 2008–2025.

B. Albrecht, Rosenstiel School of Marine and Atmospheric Sciences, University of Miami, Miami, FL 33149–1098, USA.

P. Kollias, Atmospheric Science Department, Brookhaven National Laboratory, Upton, NY 11973, USA. (pkollias@bnl.gov)